Hardin, R.A., and Beckermann, C., "Simulations of the Effect of Section Size and Cooling on Sigma Phase Formation in Duplex Stainless Steels," in Proceedings of the 66th SFSA Technical and Operating Conference, Paper No. 3.6, Steel Founders' Society of America, Chicago, IL, 2012.

Simulations of the Effect of Section Size and Cooling on Sigma Phase Formation in Duplex Stainless Steels

Richard A. Hardin and Christoph Beckermann

Department of Mechanical and Industrial Engineering
The University of Iowa, Iowa City, IA 52242

Abstract

In this study the effects of section size and cooling process parameters on sigma (σ) phase formation in duplex stainless steels CD3MN and CD3MWCuN are investigated by comparing cooling simulation results to σ phase TTT/CCT transformation diagrams for the alloys. The effect of section size on the depth into the section at which σ phase begins to form is explored by examining two cases of cylindrical sections having 30 inch and 10 inch diameters. The effect of cooling conditions on the depth at which σ phase forms is examined by simulating the range of heat transfer coefficients typically found in the cooling or quenching stage of the heat treatment process. Four constant heat transfer coefficients h from 500 to 10,000 W/m^2°C and one surface temperature dependent heat transfer coefficient relationship are simulated and analyzed. For CD3MN, it is found the σ formation does not occur in the 30" diameter cylinder even under the least effective cooling conditions where h is 500 W/m^2°C. For CD3MWCuN and the 30" diameter cylinder section, it is found that no sigma forms until a depth of 5" below the surface under ideal cooling conditions where h is 10,000 W/m^2°C, and for the least effective cooling where h is 500 W/m^2°C it is found that no σ forms until a depth of 3.5" below the surface. Using a temperature dependent heat transfer coefficient for quenching in still water, it is found that no σ forms until a depth of 4.5" below the surface. In the case of the 10" diameter cylinder, it is found that σ formation did not occur for any of the cooling conditions or either alloy simulated.

I. INTRODUCTION

Duplex stainless steels (DSS) exhibit a desirable combination of corrosion resistance and excellent mechanical properties, such as good toughness and ductility along with high yield strength. The yield strength of DDS can be twice that of the single phase austenitic and ferrite steels, and their ductility and toughness is superior to the martensitic steels. These steels' advantageous properties, and the term "duplex", arise from their having a microstructure of two primary phases, δ-ferrite and austenite (γ) in more or less equal parts. DSS were first used in castings in the 1930s, and are ideal for many applications in the marine sector and in the chemical, gas and petroleum industries. Unfortunately, due to the high alloying contents of DSS, numerous secondary phases can form depending on composition and cooling history. These phases deteriorate the mechanical properties and corrosion resistance of DSS. In this paper, the authors use simulation to study the effect of section size and cooling conditions on the precipitation of σ phase, one of the most problematic of these secondary phases. Two cast DSS are studied, CD3MN and CD3MWCuN.

In order to achieve the duplex microstructure and good properties, castings produced from DSS are highly alloyed and carefully heat treated. During the solidification of DSS ferrite forms; which then, upon cooling, transforms into austenite in the solid state giving the desired balance between the volume fractions of the two phases. The relative amounts of the two primary phases present in DSS are determined by the composition of the alloying elements that promote the formation of ferrite or austenite, and the thermal history of the cooling process. However, below about 1000°C, there is little change that can be effected in the balance of ferrite and austenite in DSS. The main alloying elements adjusted to affect the ferrite-austenite phase balance in DSS are Cr, Mo, Ni, N, Si, C and Mn. To demonstrate which elements promote the formation of which phase, it is illustrative to examine an empirical correlation between the amounts of alloying elements and the resulting ferrite percentage (wt%) in the duplex microstructure. One such correlation is given by [1]

$$\begin{aligned} \mathrm{Cr_{eq}} &= \%\mathrm{Cr} + 1.73 \cdot \%\mathrm{Si} + 0.88 \cdot \%\mathrm{Mo} \\ \mathrm{Ni_{eq}} &= \%\mathrm{Ni} + 24.55 \cdot \%\mathrm{C} + 21.75 \cdot \%\mathrm{N} + 0.4 \cdot \%\mathrm{Cu} \\ \%\,\mathrm{Ferrite} &= 4.01 \cdot \mathrm{Cr_{eq}} - 5.6 \cdot \mathrm{Ni_{eq}} + 0.016 \cdot T - 20.93 \end{aligned} \tag{1}$$

where the element compositions are in wt%, and T is the annealing temperature in the range 1050°C to 1150°C. Elements in the chromium equivalent term $\mathrm{Cr_{eq}}$ are seen to promote the formation of ferrite, and $\mathrm{Cr_{eq}}$ is composed of the ferrite phase stabilizing elements Cr, Mo, and Si. In addition to these elements, Mn is also a ferrite promoter. Also in Equation (1), note that the nickel equivalent term $\mathrm{Ni_{eq}}$ reduces ferrite in the duplex microstructure and elements in $\mathrm{Ni_{eq}}$ (Ni, N, C and Cu) promote the formation of austenite. Of these elements, the desired phase balance in DSS is usually produced by adjusting Cr and Mo to affect the ferrite formation, and changing Ni and N to modify the austenite side of the balance. One will also find that correlations like Equation (1) are constructed in terms of the ratio between $\mathrm{Cr_{eq}}$ and $\mathrm{Ni_{eq}}$. In addition to chemistry, higher annealing temperatures and faster cooling rates during the ferrite to austenite transformation will result in a higher fraction of retained ferrite in the final microstructure.

An unfortunate side effect of the high alloying content of DSS is the possibility of forming numerous secondary phases, depending on composition and cooling history. These secondary phases degrade the toughness and corrosion resistance of DSS. As shown in the schematic time-temperature-transformation (TTT) diagram in Figure 1 [2], there are a variety of carbides, nitrides and intermetallic phases precipitating from approximately 1000°C to 600°C for one group of secondary phases, and from about 600°C to 300°C for another group. As the content of certain elements is increased, the TTT curves shift in the directions indicated in Figure 1. Of these secondary phases, the sigma (σ) phase is perhaps the most troublesome since it can form in relatively large amounts (up to 30 percent by volume [3]), and it has composition dependent transformation kinetics that can be relatively fast. As schematically indicated in Figure 1, the rate and amount of σ precipitation depends on the elements Cr, Mo, W, and Si. Of these, Cr and Mo have the greatest effect on σ precipitation rates and amounts. In the case of Mo, consider the TTT diagrams in Figure 2, which demonstrates the effect of molybdenum on the start of σ phase precipitation in a Fe-28 wt% Cr-Mo system [4]. The nose of the precipitation start curve moves from about 60 hours for the 2 wt% Mo steel to 6 minutes for the 5 wt% Mo steel. As schematically shown in Figure 1, the addition of Mo also shifts the TTT precipitation start curves upward. For the Fe-Cr-Mo system shown in Figure 2, the precipitation start nose is at 700°C for the 2 wt% Mo steel moving to 900°C for the 5 wt% Mo steel.

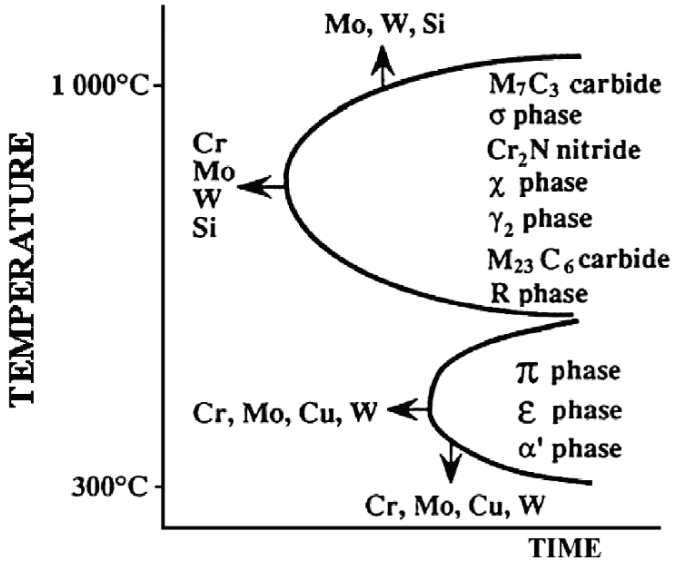

Figure 1 Schematic time-temperature transformation diagram for DSS [2] showing the two temperature ranges where secondary phases precipitate. The TTT curves will shift in the directions indicated by the arrows as the element concentrations given next to the arrowhead increase.

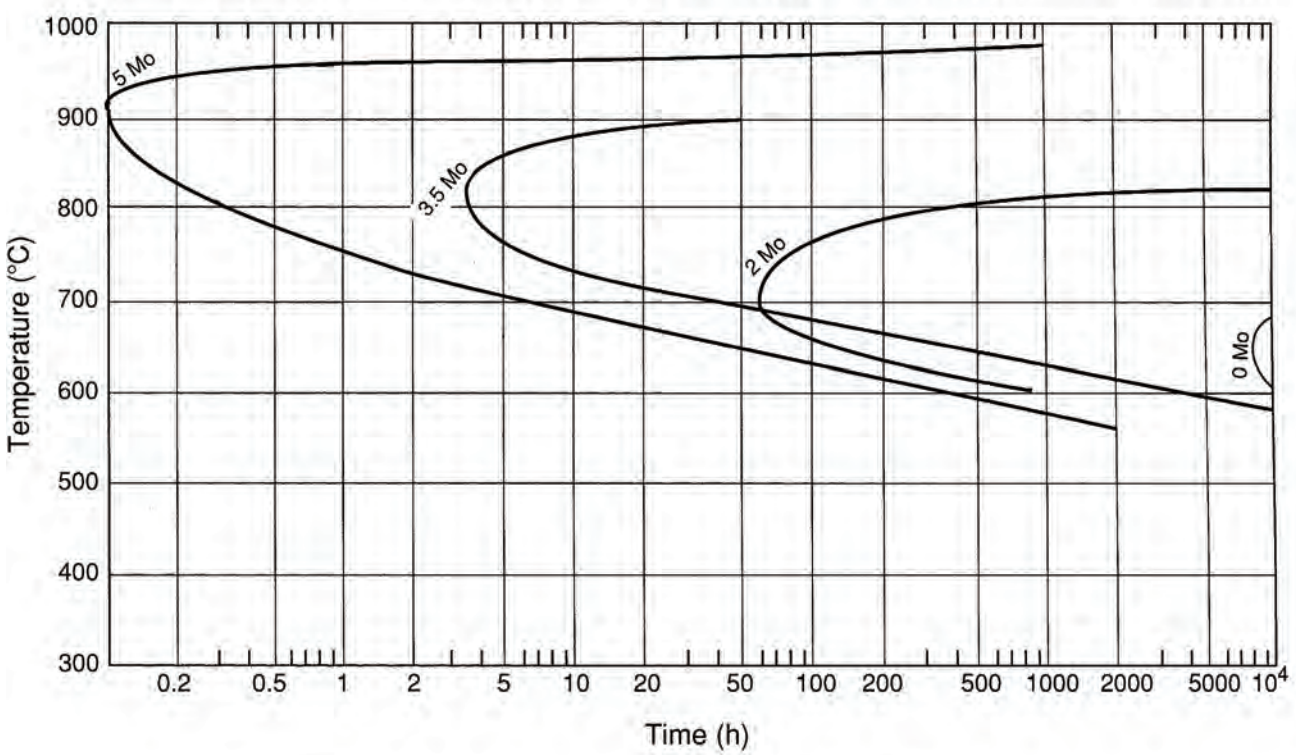

Figure 2 TTT diagrams showing the effect of molybdenum addition on start of σ phase precipitation in a Fe-28 wt% Cr-Mo system with curves for 0, 2, 3.5 and 5 wt% Mo [4].

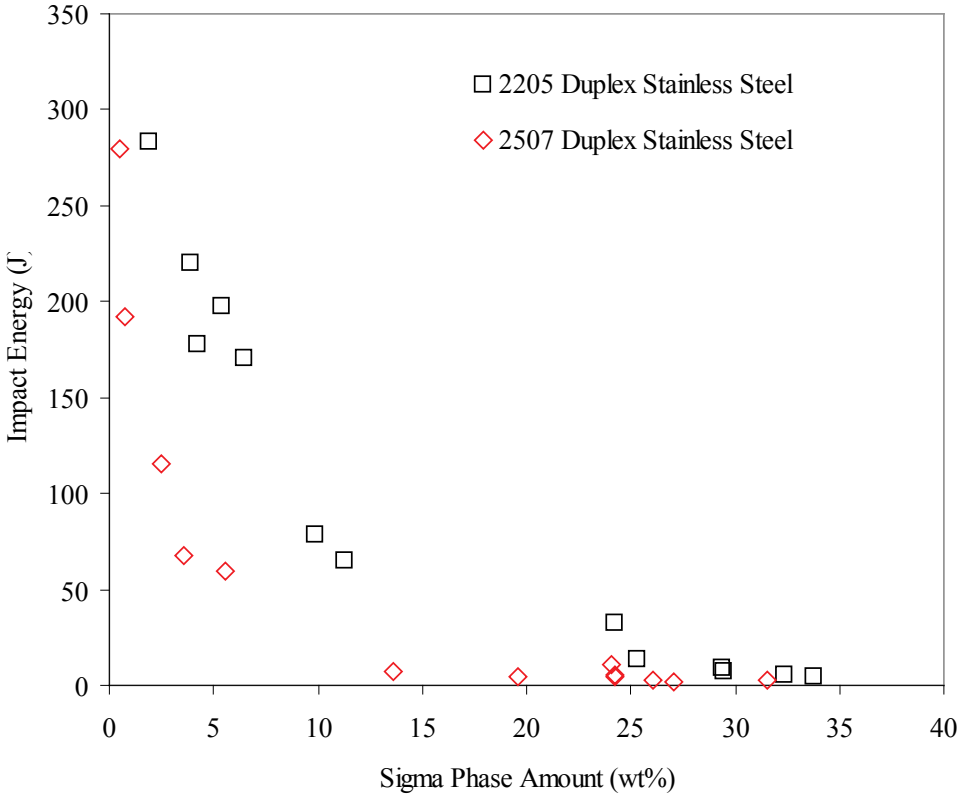

Figure 3 Results of Charpy impact testing at room temperature for wrought DSS 2205 and 2507 having σ phase amounts up to about 35 wt% (data from [5]).

As σ phase precipitates it consumes the δ-ferrite degrading the properties of DSS. It does not require a significant amount of σ phase to degrade the material properties, and this degradation is somewhat grade dependent. Consider the effect of amount of σ phase on toughness for example, shown in Figure 3, for two wrought DSS, 2205 and 2507. The grade 2205 is the wrought counterpart of the cast grade CD3MN studied in this paper. The grade 2507 is the wrought counterpart to the cast grade CE3MN, and it has the same composition as the other cast grade studied here (CD3MWCuN) except that it lacks tungsten. The impact energy in Figure 3 is progressively and nonlinearly degraded due to the embrittlement caused by the σ phase as it increases in the microstructure. In the case of the 2507 alloy, the effect of σ phase on toughness is very dramatic, requiring only a few wt% of σ phase to greatly reduce the toughness. The toughness for the 2507 grade at 3 wt% of σ phase is degraded by about 80% (about 60 J), while the 2205 grade requires 11 wt% of σ phase to reduce the toughness to that point.

Controlling the amount of σ phase precipitating in castings produced from DSS can be more challenging than in wrought products due to thick sections, and uncertain, non-uniform cooling conditions arising from the complex geometries of castings. In this study the authors were asked by the Steel Founders' Society to investigate the effects of the quenching/cooling process parameters on σ phase formation in duplex stainless steels by comparing cooling simulations to the σ phase *t-T* transformation diagrams for the alloys CD3MN and CD3MWCuN [3,6]. The primary goal of this study is to determine the depth at which σ phase begins to form for

representative sections of castings, depending on the cooling conditions for these two alloys. The effect of cooling conditions is investigated by considering a range of heat transfer coefficients h typically found in the cooling or quenching phase of the heat treatment process. The effect of section size is explored by examining two cylindrical sections having 30 inch and 10 inch diameters.

II. PROCEDURES

Kim et al. have determined σ phase time-temperature transformation diagrams for the alloys CD3MN and CD3MWCuN with chemistries given in Table 1 as specified in the range given by ASTM A890/A890M Grades 4A and 6A, respectively. Thermophysical properties for CD3MN for casting and heat transfer simulations have been determined for the chemistry specified in Table 2 [7]. Heat transfer simulation properties specifically for CD3MWCuN have not been determined. Therefore, it was decided to perform simulations using properties for the most similar grade available to CD3MWCuN that have been developed, and compare those simulation results to the CD3MN simulation results. This would indicate whether or not the chemistry differences matter. A similar alloy to CD3MWCuN from the standpoint of total alloying elements, and Fe balance, for which simulation properties have been developed, is CD4MCuN. The chemistry cast in experiments used to determine the properties of CD4MCuN is given in Table 2. Note that there are differences in the Ni, Mo, Cu and W contents between CD3MWCuN and CD4MCuN, but the balance of Fe is almost the same. In the current study, cooling simulation results for CD3MN and CD4MCuN properties will be compared.

Table 1 Chemistries from [3,6] for cast DSS whose sigma phase time-temperature transformation diagrams are given in Figures 4 and 5.

	Chemical Composition (wt%)											
Alloy	C	Mn	Si	P	S	Cr	Ni	Mo	Cu	W	N	Fe
CD3MN	0.029	0.6	0.65	0.03	0.022	22.1	5.45	2.98	0.22	0.063	0.15	67.71 (bal)
CD3MWCuN	0.034	0.59	0.87	0.02	0.011	24.5	7.33	3.62	0.67	0.76	0.23	61.36 (bal)

Table 2 Duplex alloy chemistries cast in experiments to determine the thermophysical property datasets [7].

	Chemical Composition (wt%)											
Alloy	C	Mn	Si	P	S	Cr	Ni	Mo	Cu	W	N	Fe
CD3MN	0.02	1.01	0.64	0.02	0.006	22.1	6.35	2.56	0.00	0.00	0.14	67.12 (bal)
CD4MCuN	0.022	0.76	0.59	0.02	0.001	25.7	5.76	1.84	3.00	0.00	0.15	62.16 (bal)

Two types of transformation diagrams are used to determine the degree of phase formation in heat treatment processes; the time-temperature transformation (TTT) and continuous cooling transformation (CCT) diagrams. The TTT diagram gives the rate of transformation at a constant temperature, and is determined for DSS by heating and holding samples in a range from 1050°C to 1150°C to homogenize their microstructure. Then the steel is cooled rapidly to a lower temperature, and held at that temperature while the rate of phase transformation is measured. Continuous cooling transformation (CCT) diagrams provide the extent of transformation as a

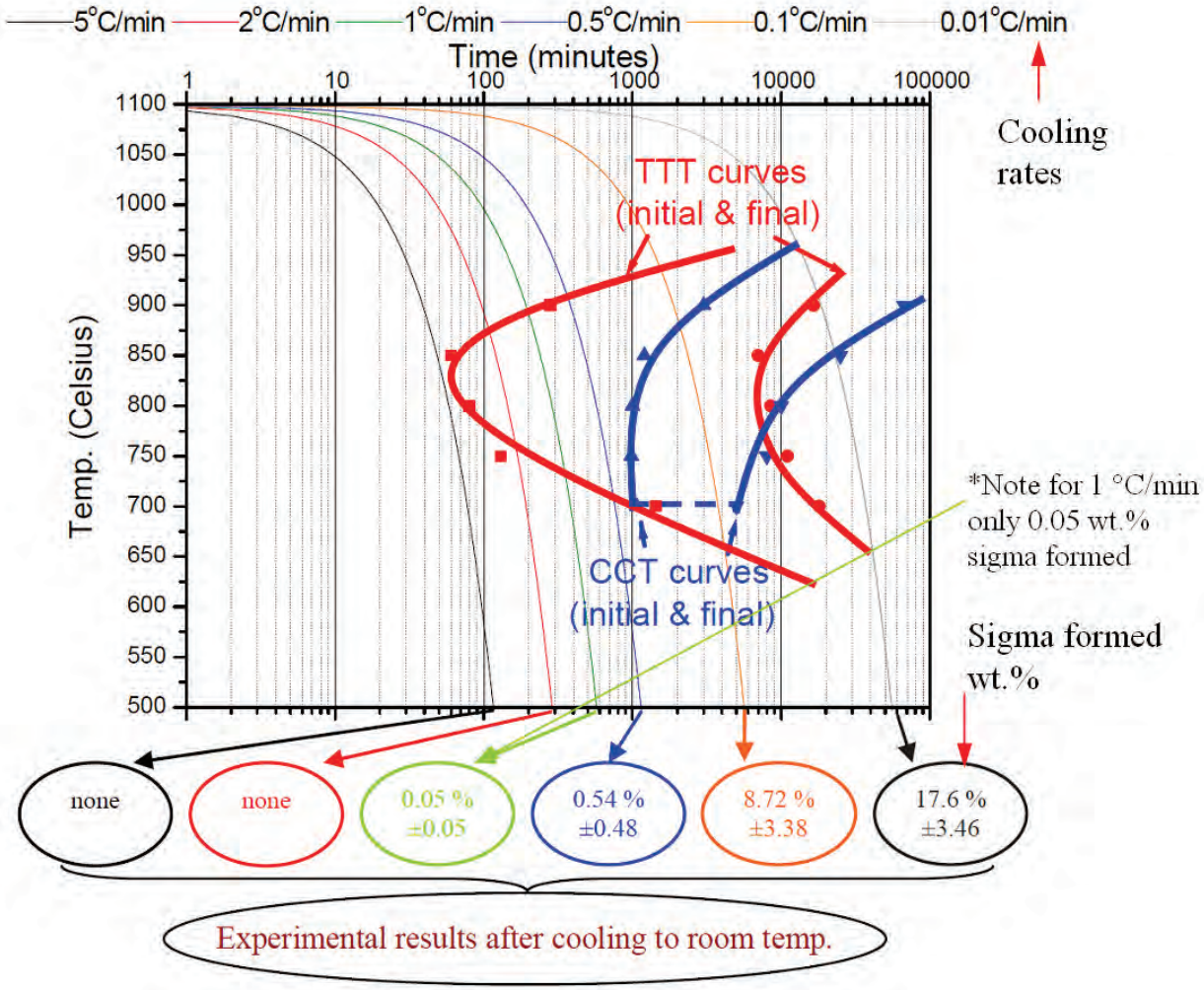

Figure 4 CD3MN duplex stainless steel TTT/CCT σ phase diagrams developed by Kim, Chumbley and Gleeson [3,6].

function of time for a continuously decreasing temperature. Here also, the steel is heated first to homogenize, but then cooled at a constant predetermined rate while the degree of transformation is measured. The development of both diagrams require numerous measurements [3,6]. The CCT diagram is applicable to heat treatment processing applications involving cooling, such as quenching. In this study both diagrams for the σ phase formation in CD3MN and CD3MWCuN will be compared with simulated cooling curves in casting sections, but the CCT diagram should be viewed as most meaningful in determining whether or not σ phase will form during the cooling process at a given point in the casting section. Avoiding the nose of the initial or start of the σ phase precipitation curve will be used to indicate whether a section is free of σ phase at a particular depth. The TTT/CCT σ phase diagrams used in this study were developed by Kim, Chumbley and Gleeson [3,6], and they are given in Figures 4 and 5.

The sigma phase transformation diagrams in Figures 4 and 5 are the original figures from the 2004 T&O paper [6]. Note that the amount of σ phase precipitated (wt%) after cooling the samples to room temperature are given in the ellipses outside the bottom- and right-side borders. In particular, for the 1 °C/min cooling rate, note that 0.05% sigma forms in CD3MN and 10.1%

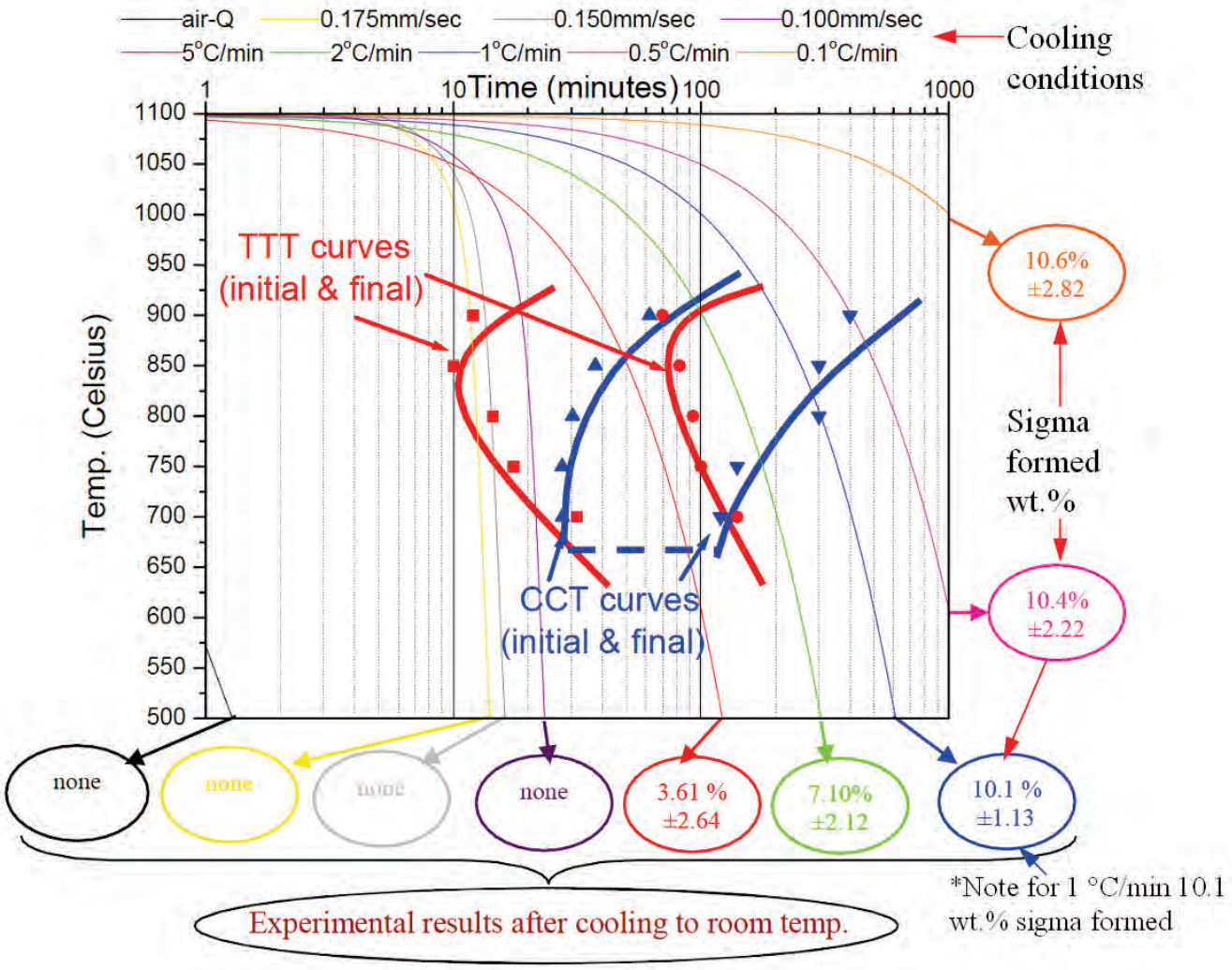

Figure 5 CD3MWCuN Duplex Stainless Steel TTT/CCT Diagrams developed by Kim, Chumbley and Gleeson [3,6].

sigma forms in CD3MWCuN, and the sigma start of transformation nose of the CCT curves lies at about 1000 minutes for CD3MN and at around 30 minutes for CD3MWCuN. As discussed in connection with Figure 1, and demonstrated in Figure 2, the shifting of the start of sigma formation to earlier times in the CD3MWCuN CCT diagram is due to the increase in Mo content compared to CD3MN. The W content of CD3MWCuN also contributes to earlier sigma phase formation. The authors have regenerated the TTT/CCT diagrams for CD3MN and CD3MWCuN in one plot in Figure 6 in order that the faster rate of σ formation in CD3MWCuN can be readily visualized; σ forms more than an order of magnitude sooner in CD3MWCuN.

As previously discussed, the differences between the thermophysical properties for these DSS will be explored by comparing cooling simulation results for CD3MN and CD4MCuN. Considering the cooling process as a time dependent heat conduction problem, the temperature evolution within the steel is described by the following energy equation

$$\rho c_p \frac{\partial T}{\partial t} = \nabla \cdot (k \nabla T) \tag{2}$$

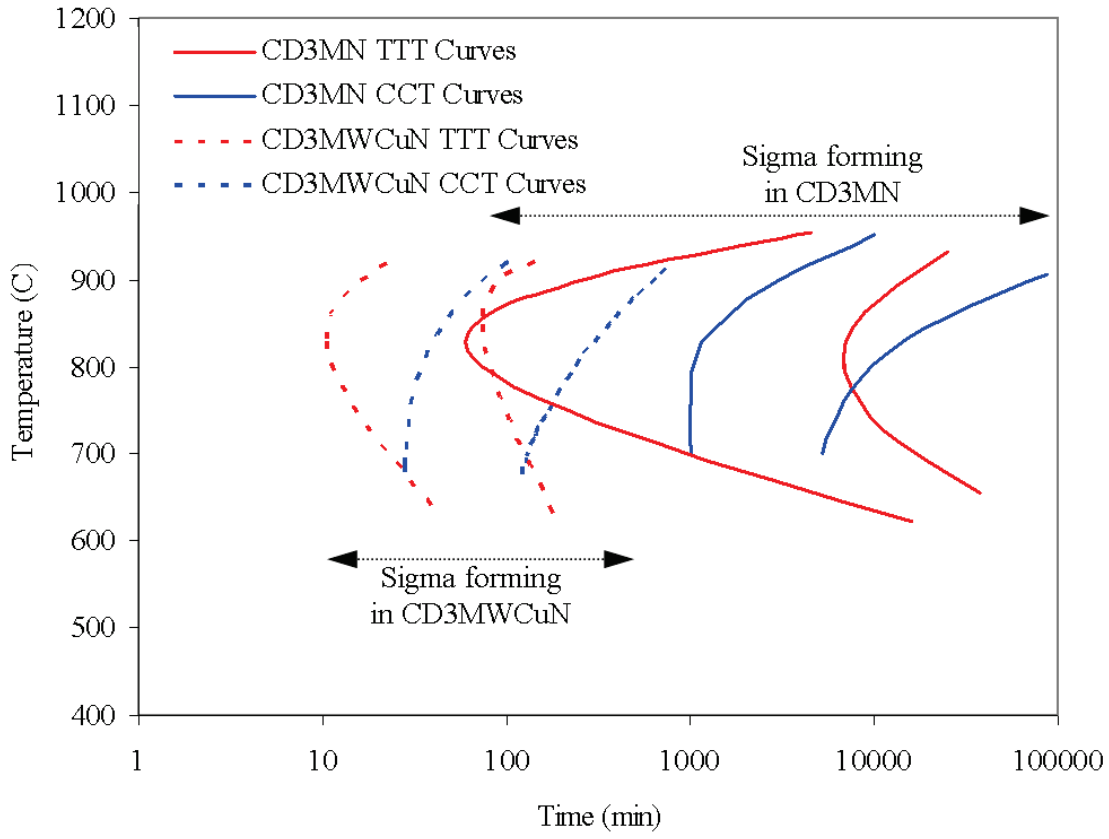

Figure 6 Comparison between CD3MN and CD3MWCuN TTT/CCT diagrams.

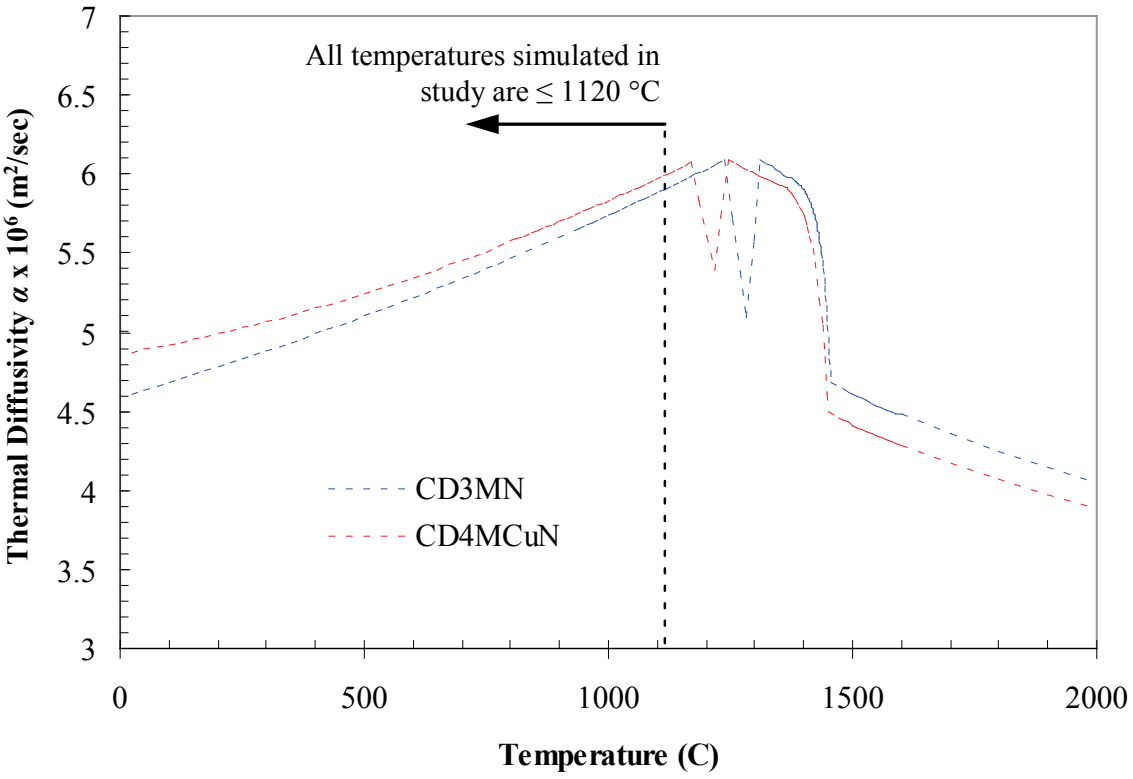

Figure 7 Comparison between thermal diffusivity α for CD3MN and CD4MCuN [7].

where t is time, ∇ is the gradient operator, and T is the temperature. The properties in Equation (2) are the density ρ, specific heat c_p and thermal conductivity k. From Equation (2) it is clear that for transient heat conduction processes, the thermal diffusivity α of the steel determines the property dependence, where α is given by

$$\alpha = \frac{k}{\rho c_P} \tag{3}$$

Therefore, to compare the differences between thermophysical property datasets of CD3MN and CD4MCuN, it is sufficient to compare the thermal diffusivities of the two alloys for this cooling process. Comparing α for CD3MN and CD4MCuN in Figure 7, the difference is not significant. In the range of interest for the heat treatment cooling process being studied, from 1120°C to room temperature, there is only about a 4% difference. Below 1120°C the thermal diffusivity α of CD4MCuN is slightly higher, which means that it will cool slightly faster than CD3MN. Uncertainties in the differences between the two alloys' cooling behavior arising from property differences are expected to be negligible compared to the uncertainties involved in the actual cooling conditions (i.e. heat transfer coefficients). Similarly, based on experience, this statement can be extended to the expected differences in α between CD3MN and CD3MWCuN.

In the simulations, the heat transfer between the surface of the casting and the cooling medium is determined by the heat transfer coefficient h and the temperature difference between them. In analyzing a heat treatment cooling process, this heat exchange is generally expressed using the Grossman number or severity of quench number H, which is defined as $H = h/2k$. The combination of the heat transfer coefficient and steel conductivity, h/k, has physical significance as it appears in analytical solutions of Equation (2) that describe the cooling process. Severity of quench numbers H for steel, and representative "average" heat transfer coefficients h, for various cooling/quenching processes and cooling assumptions are given in Table 3. The reader should understand that these are approximate and that in the actual cooling process the heat transfer is complicated by issues such as boiling, flow of the cooling medium, surface wetting and casting surface temperature dependencies. From a simulation standpoint, these complications can be addressed to a large extent by making the heat transfer coefficient a function of temperature. A classic example of such a temperature dependent h is given in Figure 8 as measured for steel quenched in still, un-agitated water. In this situation, at high temperatures a vapor layer blankets the surface and prevents good heat transfer; h is low. Then as the surface temperature decreases, the heat transfer coefficient increases to a maximum as the vapor layers become unstable and the boiling process transitions to the nucleate boiling of spherical bubbles where h is a maximum. In the current study, the temperature dependent h in Figure 8 will be used as one of the cooling conditions studied. In addition, four constant h cases will be simulated to cover a range of conditions as given in Table 3. To simulate an ideal cooling, h = 10,000 W/m^2°C is used. To simulate best possible realistic cooling, h = 4,500 W/m^2°C is used. To simulate a conservative water quench, h = 1,000 W/m^2°C is used, and to simulate a conservative oil quench, h = 500 W/m^2°C is used.

Table 3 Severity of quench number *H* and representative heat transfer coefficients *h* for steel cooling [8].

Quench Description	*H*-Value (in^{-1})	*H*-Value (m^{-1})	*h* ($Wm^{-2}°C^{-1}$)
Air still	0.02	1	28
Oil no agitation	0.2	8	276
Oil moderate agitation	0.35	14	482
Oil good agitation	0.5	20	689
Oil violent agitation	0.7	28	965
Water no agitation	1	39	1378
Water strong agitation	1.5	59	2067
Brine no agitation	2.4	94	3307
Brine violent agitation	5	197	6890

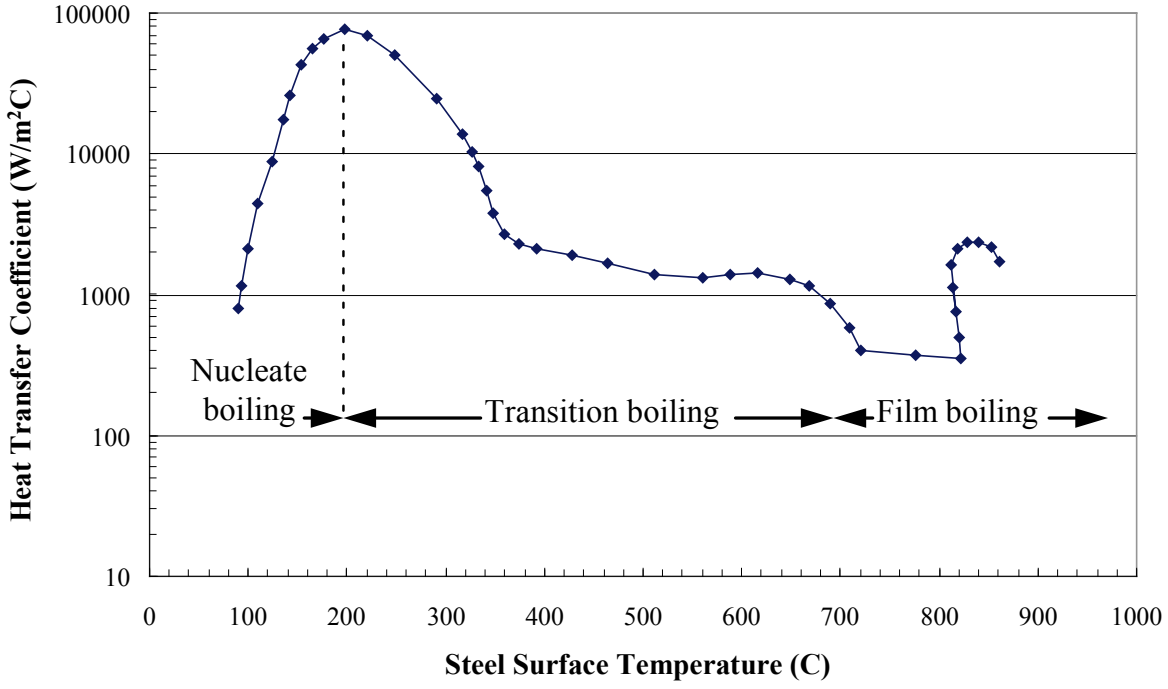

Figure 8 Measured heat transfer coefficient *h* for steel quenched in water with no agitation [8].

III. RESULTS

In Case #1 of this study shown in Figure 9, a 30” diameter cylinder is cooled in a 25°C medium from an initial annealing temperature of 1120°C. Simulations are performed using *MAGMAsoft* with properties from [7] for CD3MN and CD4MCuN. The first set of simulations presented here are for ideal cooling condition using h = 10,000 W/m^{2}C and compare the cooling simulation results using the thermophysical property datasets for CD3MN and CD4MCuN. This comparison will test whether the thermophysical properties affect the results enough to be of concern. The ends of the cylinder are perfectly insulted to prevent axial conduction, and the resulting heat transfer is in the radial direction only. Sections of temperature contours on the mid-plane between the two ends of the cylindrical simulation domain are shown in Figure 10 for the CD3MN alloy at five points in time from 30 seconds to 1 hour 40 minutes from the start of cooling. The temperature contours are concentric rings, as expected from the boundary conditions. Temperature versus time cooling curves for the sixteen virtual thermocouples placed at 1” intervals from the center to the surface are given in Figure 11 for CD3MN. For this ideal cooling case, the differences between the temperature time curves at all the virtual thermocouples were almost imperceptible for the two alloy property datasets (plotted in Figure 7). All the cooling conditions were simulated for both alloy datasets, and for each cooling condition the temperature versus time curves for the two alloys show very little difference. This can be seen at two of the virtual thermocouple locations for all cooling conditions in Figure 12(a) at 1” from the cylinder surface and in Figure 12(b) at the center of the cylinder. In Figure 12, solid curves denote CD3MN properties and dashed curves CD4MCuN, and line colors denote cooling conditions. In Figure 12(a) there is essentially no difference between the property datasets, and at the center in Figure 12(b) there appears to be only a small effect caused by the cooling conditions on the results, and the alloy dataset used appears to have a negligible though detectable effect.

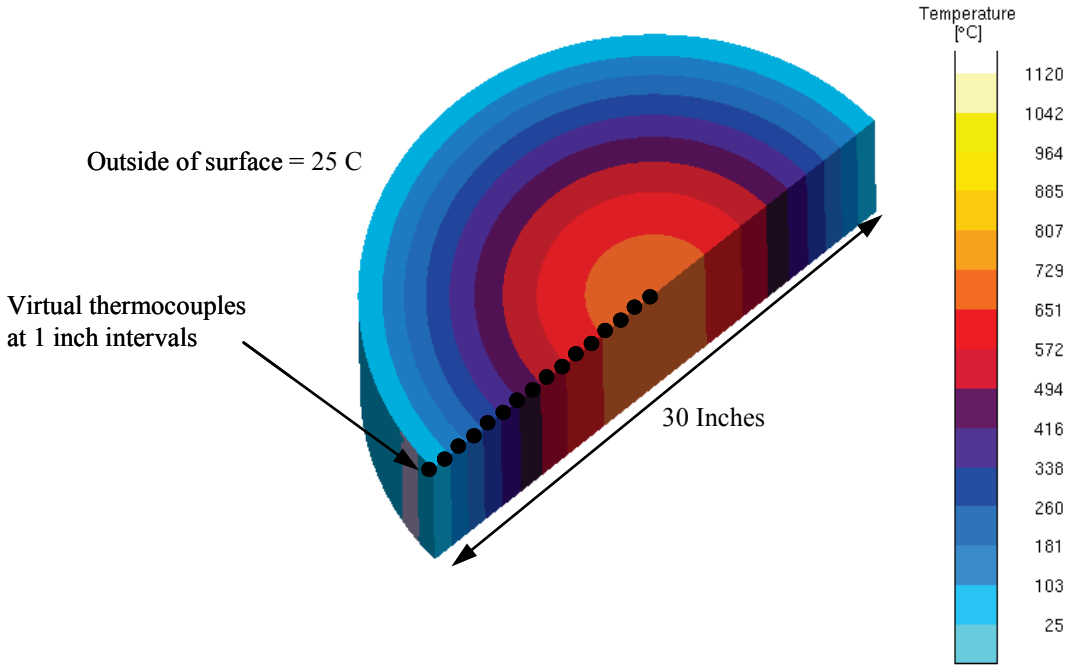

Figure 9 Case #1 for section size limit studies of sigma formation, a 10 inch diameter cylindrical section with initial temperature of 1120°C and quench bath at 25°C.

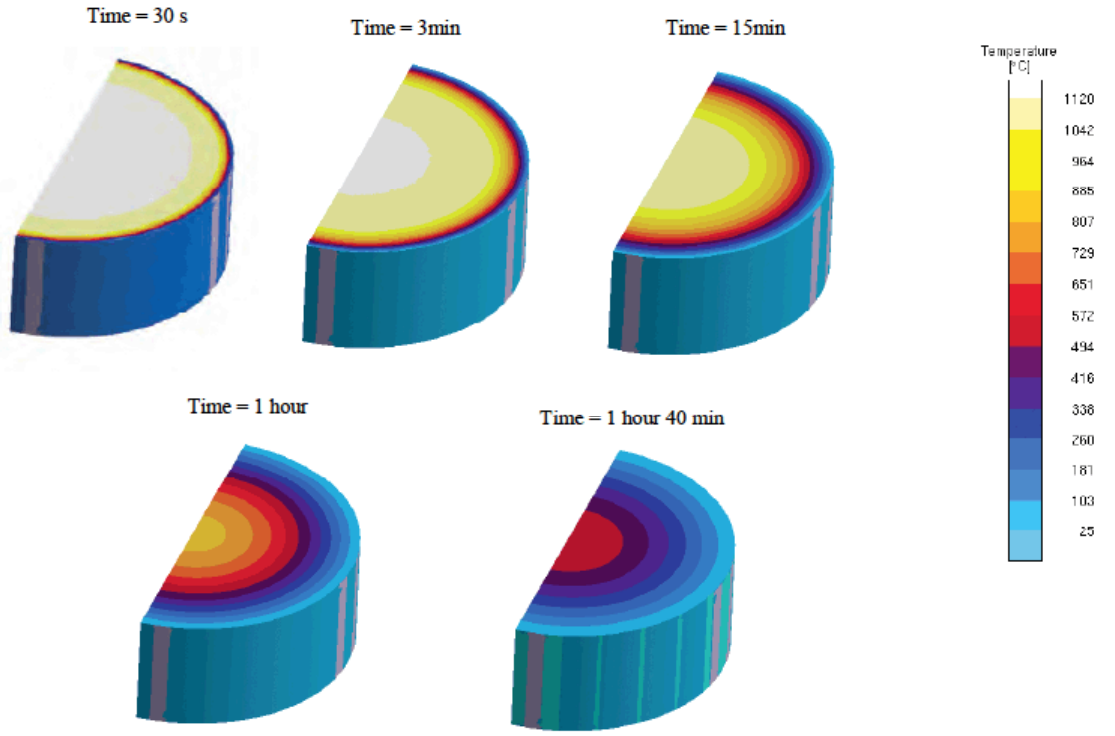

Figure 10 Temperature in section at times from start of cooling for CD3MN and h = 10,000 W/m^{2}C.

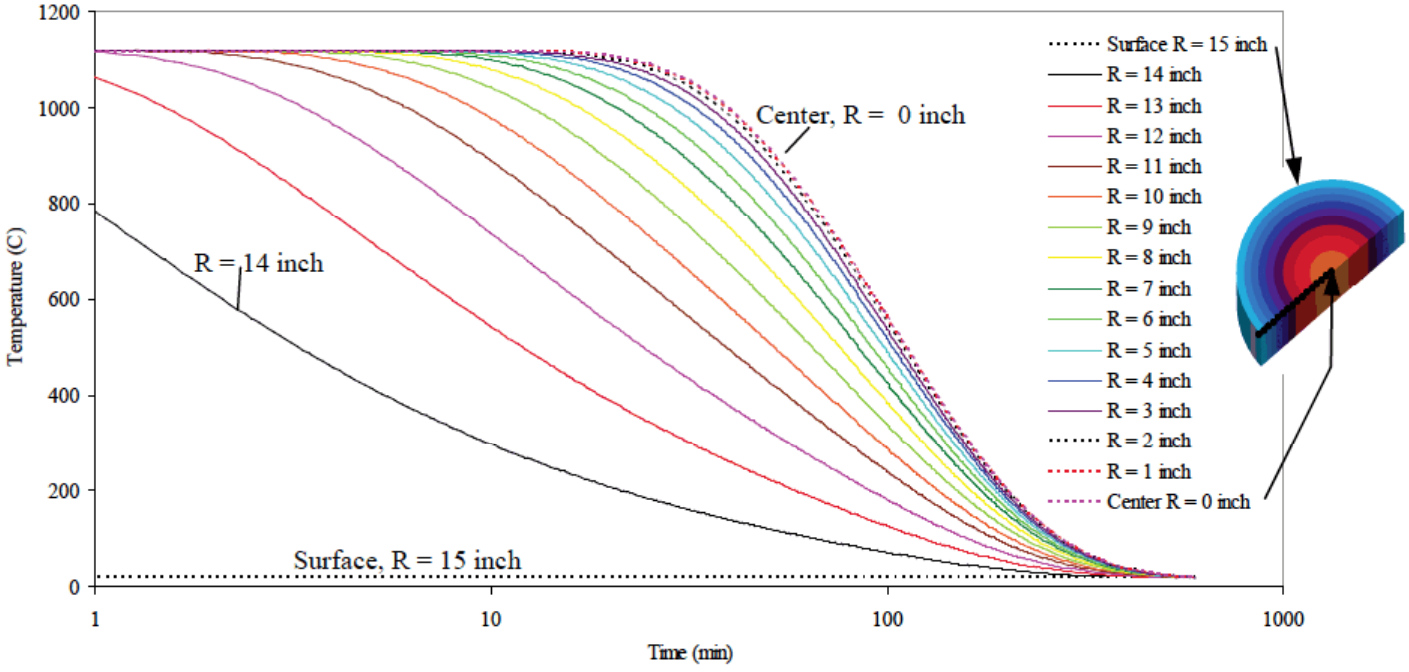

Figure 11 Temperature-time curves at thermocouples for CD3MN and h = 10,000 W/m^{2}C.

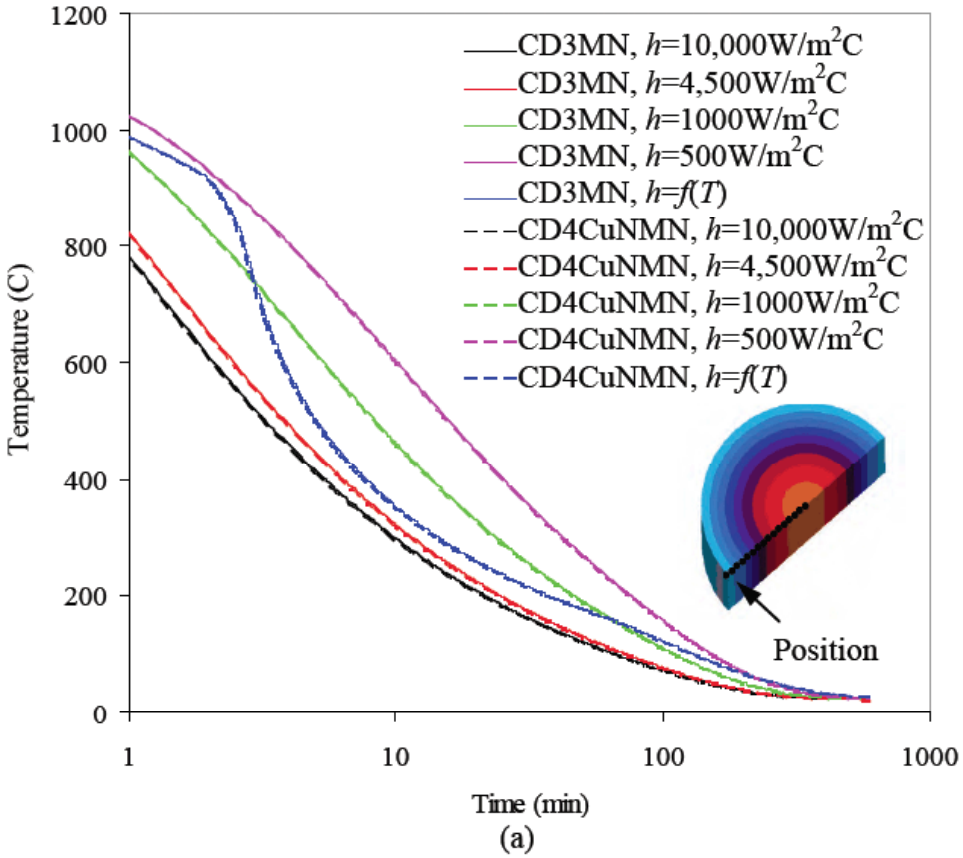

(a)

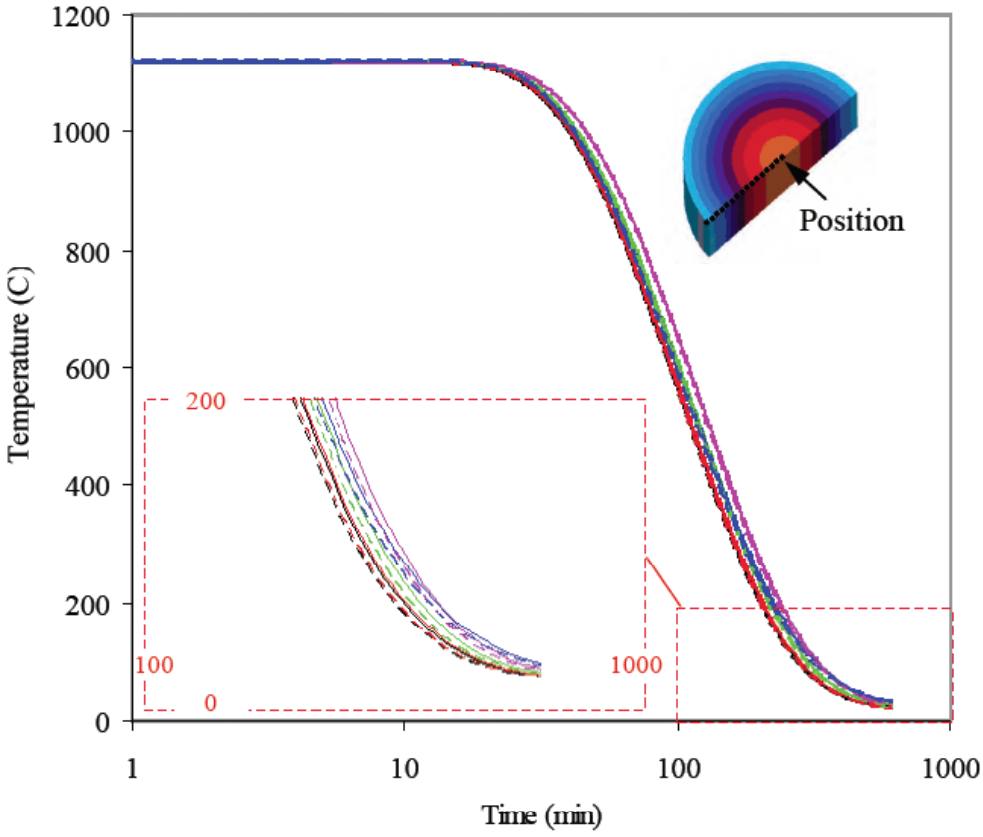

(b)

Figure 12 Curves at virtual thermocouple locations (a) 1" from surface and (b) at the cylinder center for CD3MN and CD4MCuN. Solid curves use CD3MN properties, dashed are CD4MCuN, and line colors denote cooling conditions.

After finding that the alloy property datasets appear to have a relatively minor effect on the temperature vs. time cooling curves far from the surface of the 30" diameter cylinder, results from the simulations are compared with the TTT/CCT curves for CN3MN and CD3MWCuN. Considering that the slowest cooling is at the center, it is the worst location in terms of σ precipitation. The temperature-time cooling curves at the center of the 30" cylinder for the five cooling conditions are shown in Figure 13(a) for a time scale encompassing the entire cooling process and in Figure 13(b) for a time scale to 100 minutes showing detail of the σ TTT nose. The nose of the CCT curve is entirely missed with a large margin of safety. Considering these results and the CCT curve for CD3MN, it is difficult to see how σ formation can be a problem in CD3MN even for this rather large 30 inch diameter section regardless of the cooling conditions. Also, it is not necessary to run the 10 inch diameter case for this alloy, since it only cools faster and should also be free from precipitating σ.

Simulated temperature-time curves for the 30 inch cylinder are generated using the CD4MCuN property dataset for all cooling conditions. The results for the two extreme cooling conditions (h = 10,000 and 500 W/m^{2}C) are compared to the CD3MWCuN TTT/CCT curves in Figures 14 and 15, respectively. In Figure 14, using the nose of the σ precipitation start CCT curve to decide whether σ will form, it is shown that no σ forms until a depth of 5" below the surface (at a radius R=10" from the center) under ideal cooling conditions, where h is 10,000 W/m^2°C. Conversely, for the least effective cooling where h is 500 W/m^2°C in Figure 15, it is found that no σ forms at a depth of 3.5" below the surface (at a radius R=11.5" from the center) according to the simulated cooling curves. For the temperature dependent heat transfer coefficient cooling condition (recall from Figure 8) it is found that the σ free depth is predicted to be 4.5" below the surface (at a radius R=10.5" from the center). Since most water quench tanks are agitated, this result is a realistic though conservative estimate of the σ free depth, since no agitation was used for the data in Figure 8. It should also be mentioned that using the temperature dependent heat transfer coefficient cooling condition from Figure 8 required approximately twice the computer time since iterations are required as the temperature solution modifies the boundary condition.

The final case that remains to be presented here is for alloy CD3MWCuN using simulation Case #2, a 10" diameter cylinder section. The conditions for Case #2 are shown in Figure 17, for a 10 inch diameter cylindrical section, with virtual thermocouple data stored at 1" intervals from the center to the outer surface, with initial temperature of 1120°C and the quench bath at 25°C. Again, using the nose of the σ phase start curve from the CCT diagram for CD3MWCuN as the target for avoiding σ precipitation, it is found that σ should not precipitate in the 10 inch diameter bar for any of the cooling conditions or alloys simulated. Only the h = 500 W/m^{2}C cooling condition case is shown in Figure 18 for this case, since it is the least effective cooling condition. As seen in Figure 18, at the center of the 10 inch diameter section the nose of the CCT curve (and TTT curve for that matter) is missed by the simulation cooling curve with a large margin of error. For this case it would be surprising if σ precipitation is going to occur in this section thickness.

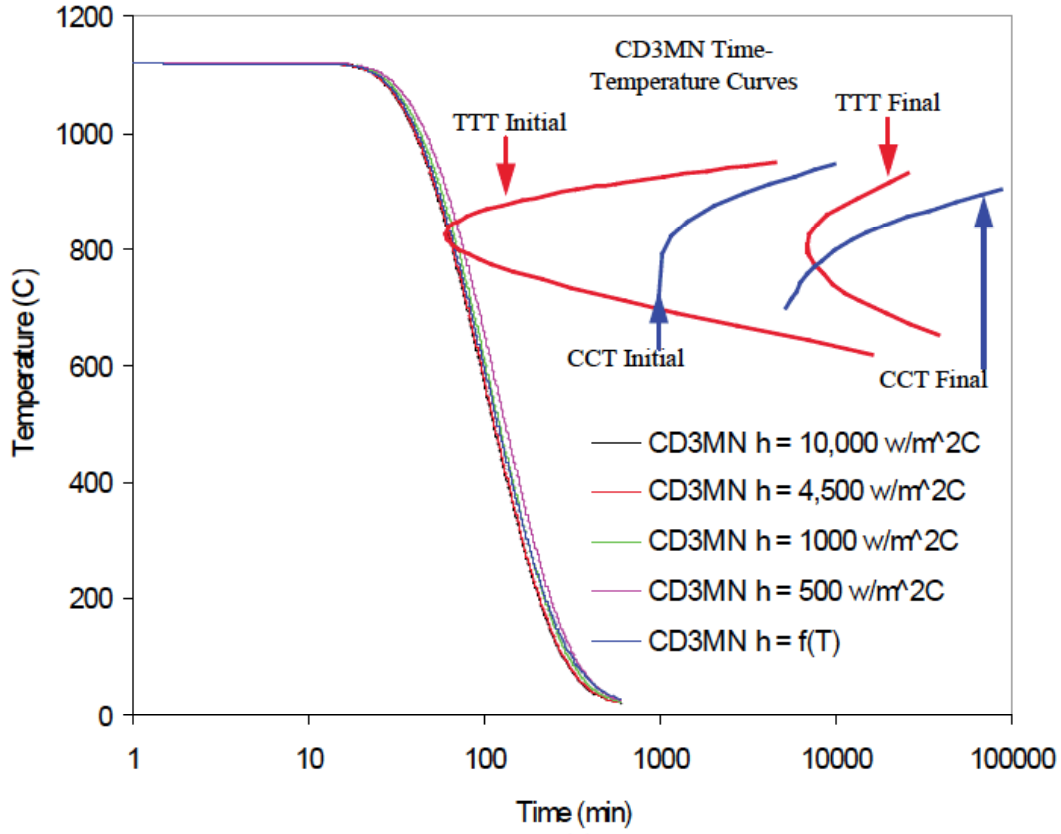

(a)

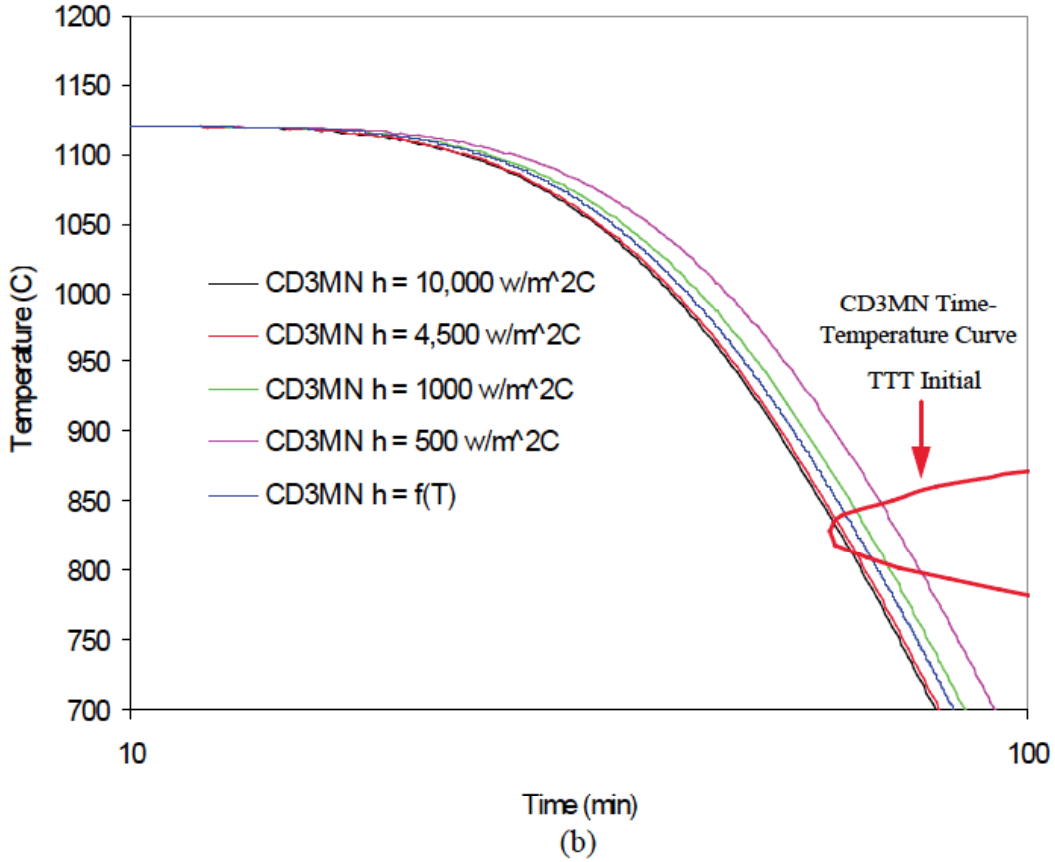

(b)

Figure 13 CD3MN time-temperature curves for the five cooling conditions at center of 30" diameter cylinder for (a) time scale encompassing the entire cooling process and (b) for a time scale to 100 minutes showing detail of sigma TTT nose.

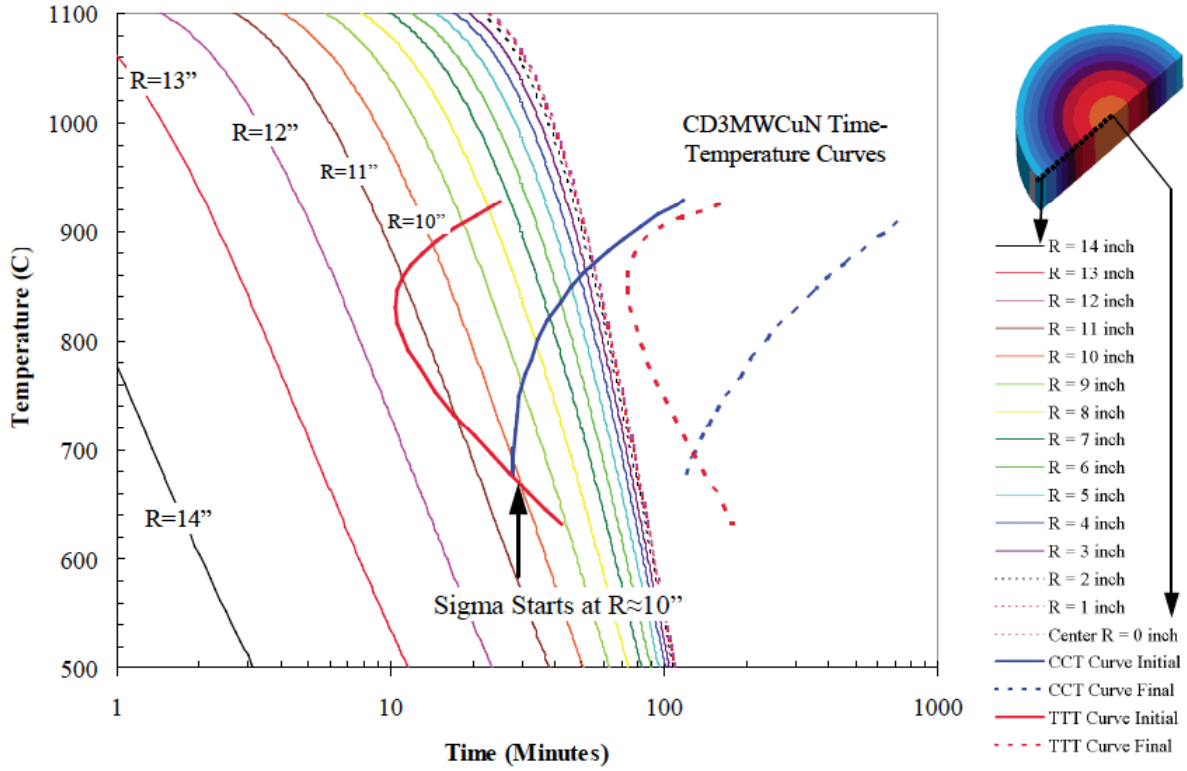

Figure 14 CD3MWCuN TTT/CCT diagrams compared with *t-T* cooling curves for with h = 10,000 W/m^{2}C; results for the best possible cooling conditions.

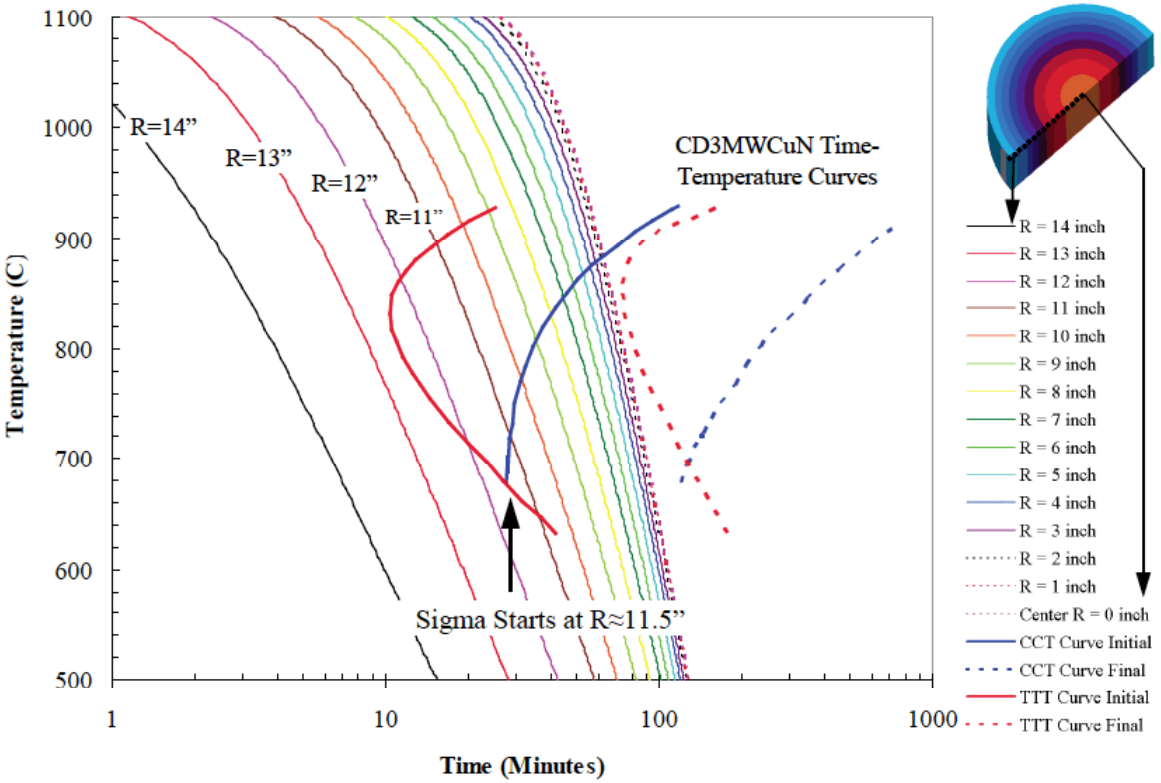

Figure 15 CD3MWCuN TTT/CCT diagrams compared with *t-T* cooling curves for with h = 500 W/m^{2}C; results representative of worst possible cooling conditions.

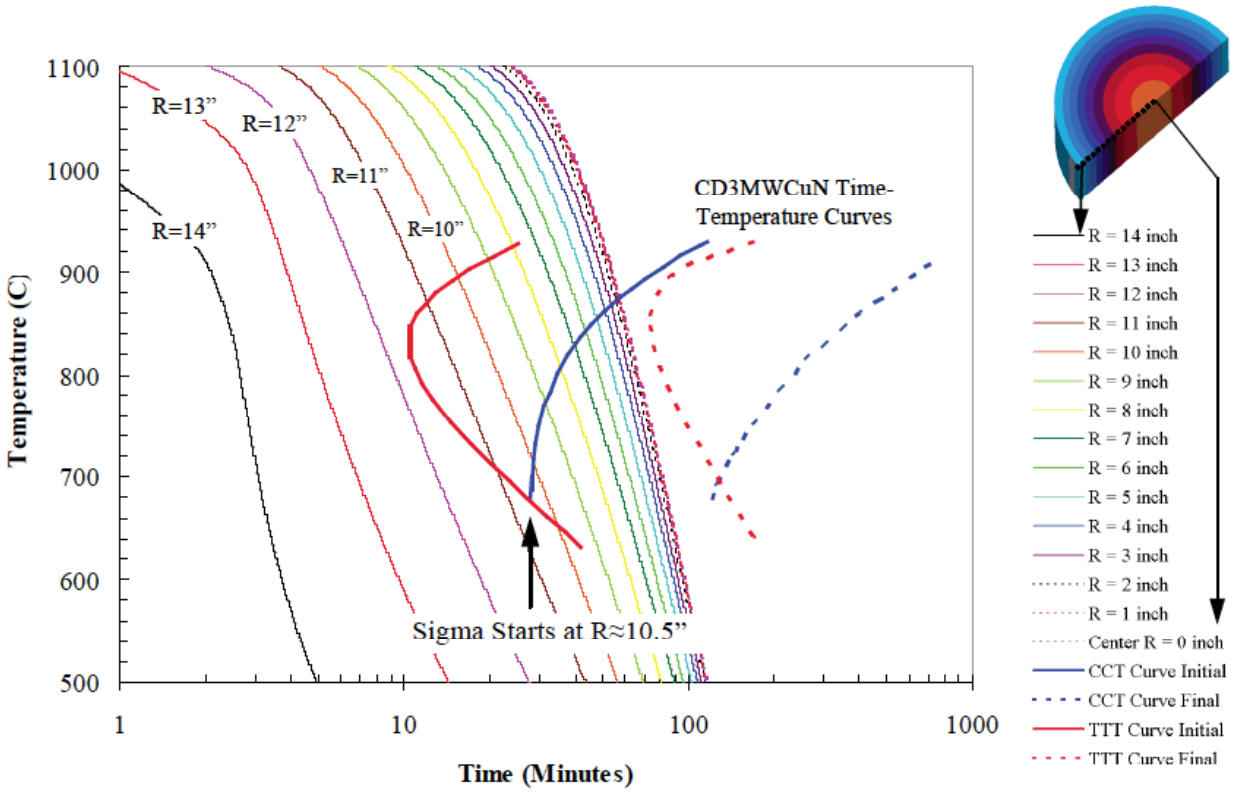

Figure 16 CD3MWCuN TTT/CCT diagrams compared with *t-T* cooling curves for with $h = f(T)$ from the un agitated water boiling curve given in Figure 7.

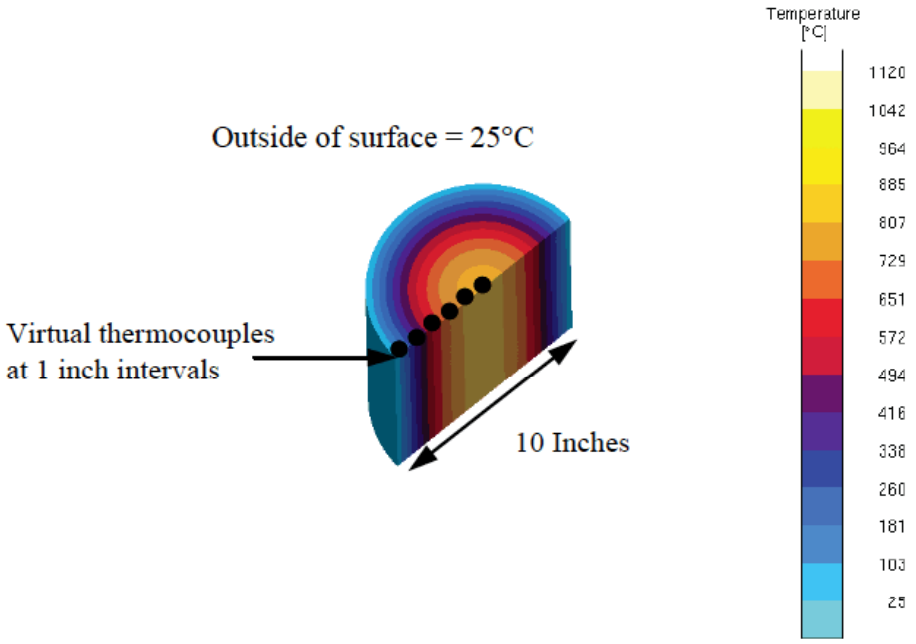

Figure 17 Case #2 for section size limit studies of sigma formation, a 10 inch diameter cylindrical section with initial temperature of 1120°C and quench bath at 25°C.

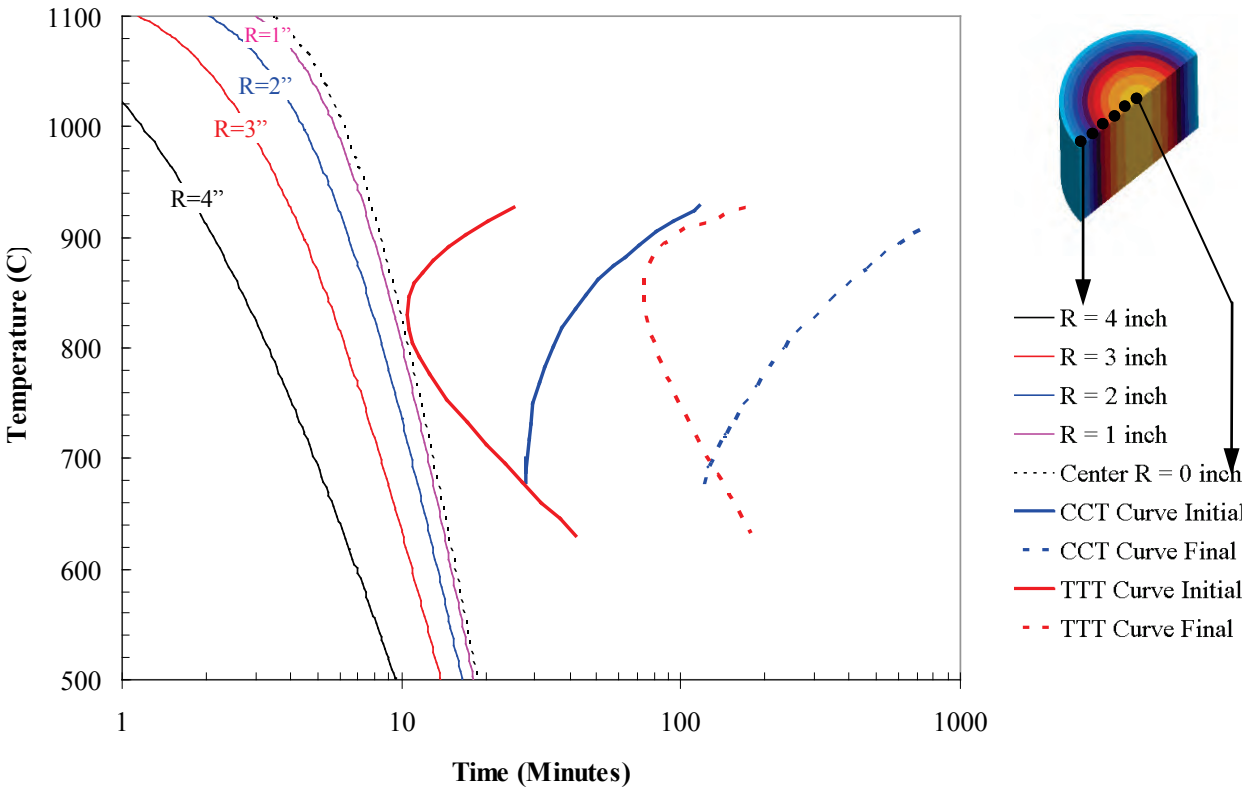

Figure 18 For Case #2 the CD3MWCuN TTT/CCT diagrams compared with *t-T* cooling curves for with h = 500 W/m^{2}C; results are representative of least effective cooling condition studied here.

IV. CONCLUSIONS

In this brief study, the effect of quenching/cooling process parameters on σ phase formation in the duplex stainless steels CD3MN and CD3MWCUN has been studied by comparing CCT diagrams and heat transfer simulation results. The role of section size on the depth at which σ phase begins to form for alloy and cooling conditions is investigated by simulating two cases, the cooling of 30 inch and 10 inch diameter cylinders. Cooling conditions have been investigated by simulating the range of heat transfer coefficients typically found in the cooling or quenching stage of the heat treatment process. Simulations using four constant heat transfer coefficients and a surface temperature dependent heat transfer coefficient have been performed.

It was found that, for CD3MN, σ formation does not occur in the 30" diameter cylinder even under the least effective cooling conditions where h is 500 W/m^2°C. For the 30" diameter cylinder section and CD3MWCuN, it was found that no σ forms until a depth of 5" below the surface under ideal cooling conditions, where h is 10,000 W/m^2°C, and for the least effective cooling it was found that no σ forms until a depth of 3.5" below the surface. For the 30 inch cylinder simulated using the still water quench heat transfer coefficient, it was found that no σ forms until a depth of 4.5" below the surface. Finally, for all 10 inch diameter cylinder simulations, it was found that σ formation did not occur for any of the cooling conditions or either alloy simulated.

This study demonstrates how simulation results can be used with CCT diagrams to investigate whether sections and areas of the casting are susceptible to σ precipitation and the mechanical and corrosion property degradation that accompanies it. This investigation was performed outside of any formal research program. Nonetheless it serves to begin to address some important issues in the heat treatment of duplex stainless steel casting, and demonstrates a methodology to study these issues in more detail in the future.

ACKNOWLEDGEMENTS

The authors acknowledge the Steel Founders' Society of America for their input and interest in pursuing this study. In particular, Malcolm Blair should be recognized for throwing down the gauntlet to us, challenging us to investigate this area, just as he has challenged researchers to pursue so many topics over the years to advance the steel foundry industry. We wish him a healthy and happy retirement; cycling in the finest weather with a strong tailwind. Malcolm's experience, insight and guidance will be sorely missed.

REFERENCES

1. International Molybdenum Association (IMOA), *Practical Guidelines for the Fabrication of Duplex Stainless Steels*, IMOA, London, UK, 2009, pp. 10.
2. Charles J., "The Duplex Stainless Steels: Materials to Meet Your Needs," Proceedings of the Conference *Duplex Stainless Steels '91*, Beaune, France, 1991, vol. 1, pp.3-48.
3. Kim Y., Chumbley L. S., and Gleeson B, "Determination of Isothermal Transformation Diagrams for Sigma-Phase Formation in Cast Duplex Stainless Steels CD3MN and CD3MWCuN," Metall. Mater. Trans. A, Vol. 35A, 2004, pp. 3377-3386.
4. *Steel Heat Treatment: Metallurgy and Technologies*, G. E. Totten editor, Taylor & Francis, Boca Raton, FL, 2007, p.715.
5. Topolska S., Łabanowski J., "Effect of Microstructure on Impact Toughness of Duplex and Superduplex Stainless Steels," J. of Ach. in Mat. and Man. Eng., 2009, 36(2), pp. 142-149.
6. Kim Y., Chumbley S. and Gleeson B., "Transformation Diagrams of Intermetallic Phase Precipitation in Cast Duplex Stainless Steels CD3MN and CD3MWCuN," in Proceedings of the 58th SFSA Technical and Operating Conference, Paper No. 3.4, Steel Founders' Society of America, Chicago, IL, 2004.
7. Carlson, K.D., and Beckermann, C., "Determination of Solid Fraction-Temperature Relation and Latent Heat Using Full Scale Casting Experiments: Application to Corrosion Resistant Steels and Nickel Based Alloys," Int. J. Cast Metals Research, Vol. 25, 2012, pp. 75-92.
8. Totten G. E., Bates C.E., and Clinton N.A., *Handbook of Quenchants and Quenching* Technology, ASM International, Materials Park, OH, 1993.